Cerebellar Purkinje cells can differentially modulate coherence between sensory and motor cortex depending on region and behavior

Sander Lindeman[1,5], Lieke Kros[1,5], Sungho Hong[2], Jorge F. Mejias[3], Vincenzo Romano[1], Mario Negrello[1*], Laurens W.J. Bosman[1*] and Chris I. De Zeeuw[1,4]

[1]*Department of Neuroscience, Erasmus MC, 3015 GE Rotterdam, the Netherlands*

[2]*Computational Neuroscience Unit, Okinawa Institute of Science and Technology, 1919-1 Tancha, Okinawa 904-0495, Japan*

[3]*Swammerdam Institute for Life Science, University of Amsterdam, 1090 GE Amsterdam, the Netherlands*

[4]*Netherlands Institute for Neuroscience, Royal Academy of Arts and Sciences, 1105 BA Amsterdam, the Netherlands*

[5]*These authors contributed equally*

**Correspondence to Laurens Bosman, Department of Neuroscience, Erasmus MC, PO Box 2040, 3000 CA Rotterdam, The Netherlands, Email: l.bosman@erasmusmc.nl;*

or to Mario Negrello, Department of Neuroscience, Erasmus MC, PO Box 2040, 3000 CA Rotterdam, The Netherlands, Email: m.negrello@erasmusmc.nl

ABSTRACT

Coherence among sensory and motor cortices is indicative of binding of critical functions in perception, motor planning, action and sleep. Evidence is emerging that the cerebellum can impose coherence between cortical areas, but how and when it does so is unclear. Here, we studied coherence between primary somatosensory (S1) and motor (M1) cortices during sensory stimulation of the whiskers in the presence and absence of optogenetic stimulation of cerebellar Purkinje cells in awake mice. Purkinje cell activation enhanced and reduced sensory-induced S1-M1 coherence in the theta and gamma bands, respectively. This impact only occurred when Purkinje cell stimulation was given simultaneously with sensory stimulation; a 20 ms delay was sufficient to alleviate its impact, suggesting the existence of a fast, cerebellar sensory pathway to S1 and M1. The suppression of gamma band coherence upon Purkinje cell stimulation was significantly stronger during trials with relatively large whisker movements, whereas the theta band changes did not show this correlation. In line with the anatomical distribution of the simple spike and complex spike responses to whisker stimulation, this suppression also occurred following focal stimulation of medial crus 2, but not of lateral crus 1. Granger causality analyses and computational modeling of the involved networks suggest that Purkinje cells control S1-M1 coherence most prominently via the ventrolateral thalamus and M1. Our results indicate that coherences between sensory and motor cortices in different frequency ranges can be dynamically modulated by cerebellar input, and that the modulation depends on the behavioral context and is site-specific.

Keywords

Cerebellum, cerebral cortex, whisker system, laminar model, LFP

Author Contributions

S.L., S.H., J.F.M., M.N., L.W.J.B. and C.I.D.Z. designed research; J.F.M. designed and executed computational model, S.L., L.K., V.R. and L.W.J.B. performed biological experiments; S.L., L.K., S.H., J.F.M., V.R., M.N., L.W.J.B. and C.I.D.Z. analyzed data; S.L., L.W.J.B. and C.I.D.Z. wrote the paper with contributions from all authors.

Significance Statement

Coherent activity between sensory and motor areas is essential in sensorimotor integration. We show here that the cerebellum can differentially affect cortical theta and gamma band coherences evoked by whisker stimulation via a fast ascending and predictive pathway. In line with the functional heterogeneity of its modular organization, the impact of the cerebellum is region-specific and tuned to ongoing motor responses. These data highlight site-specific and context-dependent interactions between the cerebellum and the cerebral cortex that can come into play during a plethora of sensorimotor functions.

INTRODUCTION

Coherent oscillations can bind different brain areas by affecting susceptibility of neurons to synaptic input and providing a timing mechanism for generating a common dynamical frame for cortical operations (1, 2). For example, coherence can create a temporal framework for concerted neural activity that facilitates integration of the activity of sensory and motor areas (3-5). Online integration is particularly relevant, when animals, including ourselves, explore their environment via active touch, requiring sensory input to be directly related to the momentary position and movement of eyes, fingertips, antennae, whiskers or other organs (6-8).

Coherence often occurs in specific frequency bands that can be associated with different functions. In the field of sensorimotor integration, skilled movements rely on intercortical coherence between sensory and motor areas that occur in the theta (4-8 Hz) range during force generation, while coherence at higher bands is engaged during the preparation thereof (9). Likewise, within the field of visual perception, coherence in the alpha (8-12 Hz) and gamma (30-100 Hz) bands have been found to contribute to feedback and feedforward processing, respectively (10, 11).

The appearance of coherence among different cortical regions implicates reciprocal connections between neurons distributed among different layers within the cerebral cortex (12-16) as well as inputs from subcortical structures like the thalamus (17-20) (Fig. 1A). Accordingly, one of the main inputs to the thalamus, i.e., the cerebellum, has a strong impact in organizing cortico-cortical coherence (21-23). Indeed, disruption of cerebellar function, whether inflicted pharmacologically in rats (22) or due to stroke in patients (21), affects cortico-cortical coherence.

Even though the impact of cerebellar activity on cortical coherence is well established (22, 24, 25), it remains to be elucidated to what extent and how the cerebellum can differentially influence different frequency bands, to what extent such potentially different impacts depend on the behavioral context, and whether these differential effects are mediated through different cerebellar modules (26-28). Here, we set out to address these questions by investigating the impact of Purkinje cell activity on coherence between the whisker areas of the primary somatosensory (wS1) and motor cortex (wM1) during stimulation of the whiskers in awake behaving mice. When we stimulated Purkinje cells optogenetically at different intervals with respect to air puff stimulation of the whiskers, we observed that these main output neurons differentially contribute to wS1-wM1 theta and gamma band coherences with opposite effects, depending on ongoing behavior and their precise site in the cerebellar hemispheres.

RESULTS

Purkinje cell stimulation modulates sensory responses in wS1 and wM1

Whisker stimulation triggers fast responses in wS1 and wM1 (29-31) as well as in the cerebellar cortex (28, 32, 33). Before studying the impact of cerebellar stimulation on the cortical coherence between wS1 and wM1, we first needed to determine to what extent the individual cortical responses within wS1 and wM1 depended on cerebellar activity.

Thereto, we compared local field potentials (LFPs) in wS1 during whisker stimulation in the absence or presence of optogenetic stimulation of Purkinje cells in the crus 1 and crus 2 area (Figs. 1B, S1). Air puffs applied to the whiskers evoked canonical LFP responses in wS1 in that they induced an initial fast decrease, first in layer IV and then also in the superficial and deep layers, followed by increased LFP signals (Figs. 1C, S2A, S3A). Decreases in LFP signal have been suggested to correspond with increased neuronal excitation (34), returned to baseline after roughly 200 ms.

Given the strong and direct trigemino-thalamo-cortical pathways (8, 35), a significant impact of Purkinje cell stimulation during whisker stimulation on the initial response in the input layer of wS1 would not be expected. Indeed, this was not the case (p = 0.197, Fig. S4A; see Table S1 for details on statistical analysis). However, the spread of excitation to the deeper layers was enhanced by Purkinje cell stimulation (p = 0.012, Fig. S4A). Likewise, Purkinje cell stimulation reduced the positive LFP peak in the deeper layers (p = 0.024, Figs. 1E-F, S2A, S3A). Both effects were not observed when we postponed the Purkinje cell stimulation 20 ms relative to the whisker stimulation (Figs. 1G-H, S2A, S3A, S4A, Table S1). When we, as a control, stimulated the Purkinje cells in the absence of sensory stimulation, we observed that this induced a near-complete block of the output of cerebellar nucleus neurons, followed by rebound firing at the end of the 100 ms stimulus interval (Fig. S2B). Of note, the period of silencing led to a small, but observable increase in neural activity in wS1 (negative LFP) while the rebound firing in the cerebellar nuclei correlated with decreased neural activity in wS1 (positive LFP; Fig. 1D), suggesting that the connection between cerebellar nuclei and wS1 includes at least one inhibitory hub.

Similar to wS1, wM1 did not display a significant impact of Purkinje cell stimulation on the initial wave of neural excitation following sensory stimulation (Fig. S4B, Table S1). However, the subsequent positive peak in the LFP was reduced in the deeper layers (p = 0.024, Figs. 1I-L, S2A, S3B). As for wS1, this effect was abolished by a 20 ms delay between whisker and Purkinje cell simulation (Fig. 1M-N). Thus, our data indicate a fast ascending pathway via the cerebellum disinhibiting sensory responses in the deeper layers of wS1 and slightly later also in wM1.

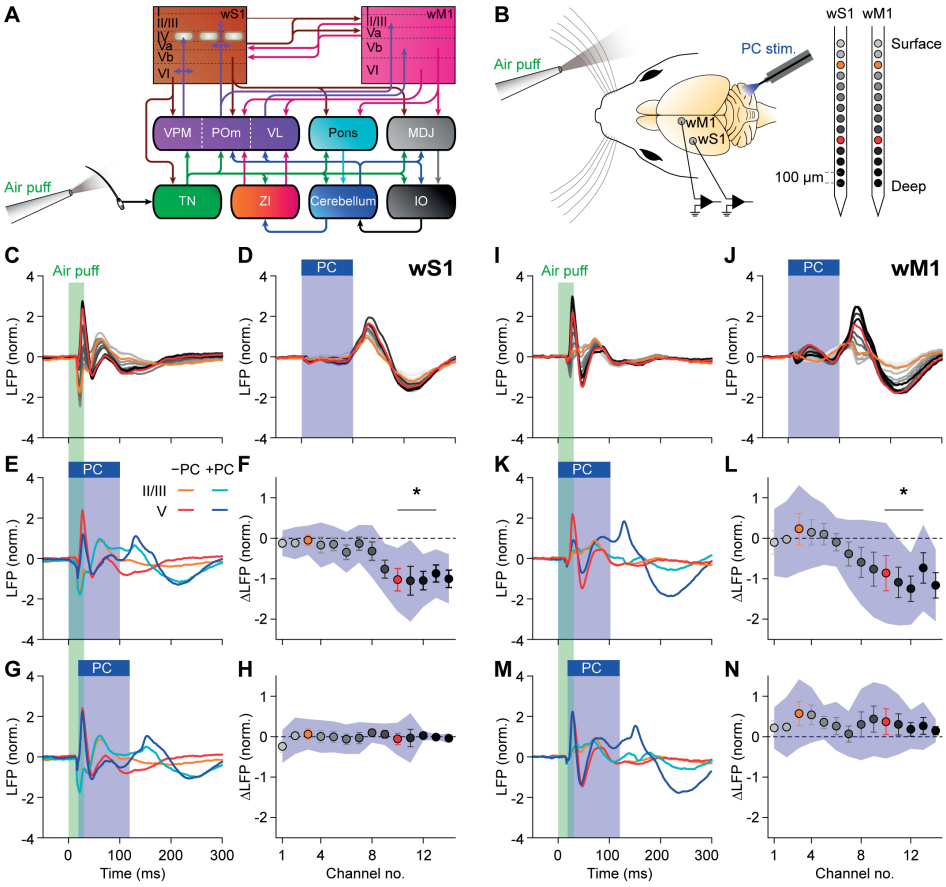

Figure 1. Purkinje cell stimulation disinhibits fast sensory responses in wS1 and wM1.

A Simplified scheme of anatomical pathways carrying whisker input to wS1, wM1 and the cerebellum, and the reciprocal cerebro-cerebral connections. IO = inferior olive; MDJ = nuclei of the mesodiencephalic junction; Pom = posterior medial nucleus; TN = trigeminal nuclei; VL = ventrolateral nucleus; VPM = ventroposterior medial nucleus; ZI = zona incerta. **B** Local field potentials (LFP) were recorded in wS1 and wM1 of awake mice using, for each area, 14 recording spots on linear silicon probes. Colors indicate their relative positions, with orange and red for the 3rd and 10th electrodes, representing the supra- and subgranular layers, respectively. Purkinje cells (PC) were stimulated optogenetically using an optic fiber with 400 µm diameter placed on the center of crus 1 (Fig. S1). **C** Whisker stimulation triggered fast responses in contralateral wS1, as illustrated by the averaged LFP traces (*n* = 100 trials per mouse, *N* = 8 mice). **D** Purkinje cell stimulation triggered delayed responses in wS1 after rebound firing in the cerebellar nuclei (Fig. S2B). **E** Comparison of the LFPs recorded during trials with whisker stimulation (orange / red) and with combined with sensory and Purkinje cell stimulation (cyan / blue). **F** During the early response period, especially the amplitude of the first positive LFP peak in the subgranular layers was affected, in addition to profound impact during later phases of sensory processing. Plotted are the averaged differences in amplitude of the first positive LFP peaks. Error bars indicate SEM and shaded area sd. **G-H** The impact of optogenetic Purkinje cell stimulation on the first positive LFP peak was largely abolished by introducing a 20 ms delay between the start of air puff sensory stimulation and the onset optogenetic Purkinje cell stimulation. **I-N** The same plots as **C-H**, but now for wM1, showing comparable impact of optogenetic Purkinje stimulation on the sensory-induced LFP signals.

Cerebellar output differentially modulates S1-M1 coherence in theta and gamma bands

As we found cerebellar activity to be able to modulate early-phase sensory responses in both wS1 and wM1, we surmised that cerebellar activity could also affect sensory-related coherent activity between these areas. As there are particularly strong connections between the subgranular layers of wS1 and the supragranular layers of wM1 (5, 36) (Fig. 1A), we initially focused on the coherence between these layers. Air puff stimulation of the whiskers triggered a fast increase in S1-M1 coherence, particularly in the beta and lower gamma band range, and to a lesser extent in the theta range (Fig. 2). Instead, whereas sensory stimulation combined with simultaneous optogenetic Purkinje cell stimulation led to a further enhancement in the sensory-induced coherence at the theta band, the same combination prominently reduced the sensory-induced coherence at the gamma band (Fig. 2A,B,E). Both of these modifications could be alleviated by delaying the optogenetic stimulation with 20 ms relative to the onset of whisker stimulation (Fig. 2A,B,E). The fact that a 20 ms lag between sensory and Purkinje cell stimulation was sufficient to, at least in part, rescue the original amplitude of sensory-evoked signals corroborates the notion that under normal physiological circumstances cerebellar modulation of cerebral coherence is probably mediated by a fast pathway. Granger causality can measure how much of the wM1 signal in a certain frequency band is controlled by the wS1 and vice versa. Applying that analysis on the sensory-induced coherence revealed that, for the comparison of the deep layers of S1 and the superficial layers of M1, both areas were involved in generation of the coherence (Fig. 2C-D).

Examining the coherence between other cortical layers, which are probably less directly coupled (Fig. 1A), we observed that the cerebellar impact broadened, now also comprising beta and higher gamma bands (Fig. S5). Granger causality analysis revealed that the sensory-induced gamma band coherence is largely triggered by the superficial layers of wS1 and from there spreads to the deep layers of wS1 (Fig. S6A-B) and the deep layers of wM1 (Fig. S6C-D). Notably, there was more balance between the deep layers of wS1 and the superficial layers of wM1 (Figs. 2C-D and S6C-D), suggesting that sensory-induced coherence is a complex phenomenon involving reciprocal connections between wS1 and wM1. The Granger causality analysis of the Purkinje cell-induced theta band coherence did not systematically reveal a strict directionality, suggesting a reciprocal involvement of wS1 and wM1.

Thus, experimentally dampening the output of the cerebellar nuclei by enhancing Purkinje cell activity results in an array of changes in sensory-induced coherences between wS1 and wM1. Effects were detected in all layers, but the most specific and reproducible changes were revealed in the comparison between theta and gamma coherence across wS1 and wM1.

Cerebellar impact on S1-M1 coherence depends on behavioral context

Air puff stimulation of the whiskers triggers reflexive protraction, the amplitude of which is correlated to cerebellar activity (28, 33). This suggests an interaction between cerebellar activ-

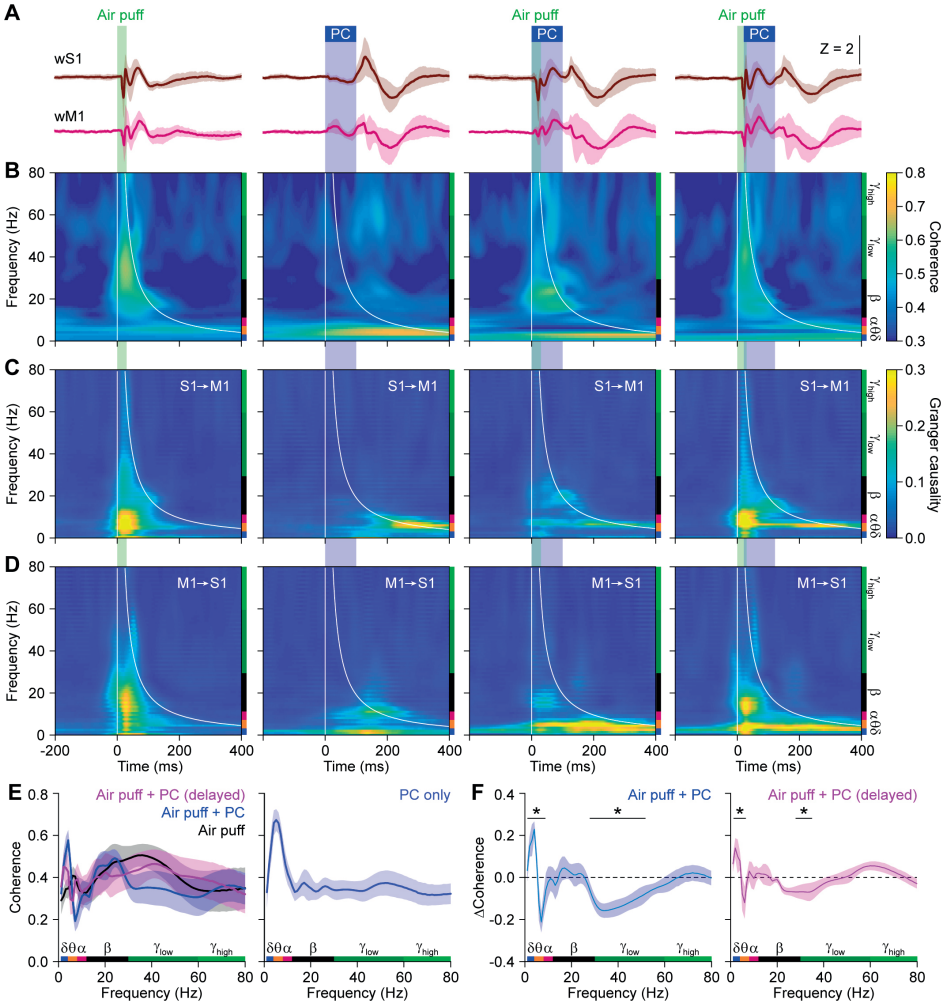

Figure 2. Reducing cerebellar output enhances and inhibits sensory-induced S1-M1 theta and gamma band coherence, respectively.

A Averaged LFP signals in subgranular wS1 and supragranular wM1 following either air puff stimulation of the contralateral facial whiskers, optogenetic Purkinje cell (PC) stimulation, or a combination of both. In the column on the right, there was a 20 ms delay between the onset of air puff and Purkinje cell stimulation. Purkinje cell stimulation was performed with an optic fiber with a 400 µm diameter placed on the center of crus 1. **B** Heat maps with the coherence strength for each frequency. Purkinje cell stimulation induced a delayed increase in the lower frequency range, mainly theta band. Sensory stimulation predominantly caused a rapid increase in the lower gamma band range. This increased coherence in the lower gamma band range could be suppressed by simultaneous optogenetic stimulation of Purkinje cells. This suppression was largely absent when the optogenetic stimuli were delayed by 20 ms, indicating the importance of fast cerebellar processing. **C** Heat maps showing Granger causality from wS1 to wM1. **D** Granger causality for wM1 to wS1. **E** Coherence after whisker stimulation (left) and for optogenetic Purkinje cell stimulation alone (right). **F** Simultaneous Purkinje cell stimulation enhanced and suppressed theta and gamma band coherence, respectively. These modulations were largely reduced by a 20 ms delay in the onset of Purkinje cell stimulation. The increased theta band activity may partly reflect a direct effect of Purkinje cell stimulation. Shaded areas indicate SEM. $N = 8$ mice; * $p < 0.05$ ($\chi^2 > 3.84$; difference of coherence test, see Methods)

ity, whisker protraction and wS1-wM1 coherence. To sharpen this statement, we singled out, for each experiment, the 50% of the trials with the largest reflexive whisker protractions and compared these to the other 50% (Fig. 3A-B). During air puff stimulation, larger protractions were correlated to lower coherence levels than smaller protractions, which was opposite during combined whisker and Purkinje cell stimulation (Fig. 3C), alluding to a significantly stronger impact of cerebellar activity during larger movements (Fig. 3D-E). Again, this impact was absent when introducing a 20 ms delay between whisker and Purkinje cell stimulation (Fig. 3D). The cerebellum therefore seems to provide contextual input with a homeostatic effect, which was particularly clear in the beta and gamma bands, but absent in the theta band. Purkinje cell stimulation in the absence of whisker stimulation did not cause a whisker movement until the end of the stimulus, as described previously (25) (Fig. S7).

Regional heterogeneity in cerebello-cerebral communication

The direction of Purkinje cell modulation upon whisker stimulation is related to the location within crus 1 and crus 2 receiving the stimulus (28). More specifically, whereas the increase in simple spike firing is most prominent in medial crus 2, that of the complex spikes, which may facilitate execution of touch-induced whisker protraction, is more robust in lateral crus 1 (28). Given this differential distribution in whisker-related Purkinje cell activity (Fig. 4A), we hypothesized that the changes in coherence described above depend on the specific area of optogenetic stimulation. To study the impact of spatial Purkinje cell stimulation on wS1 and wM1, we placed small optic fibers in a rectangular grid, targeting the medial and more lateral parts of crus 1 and crus 2. With these fibers we could reliably trigger a near-complete block of neuronal activity in the cerebellar nuclei and trigger whisker movements related to the rebound firing in these nuclei (Figs. S8 and S9). Yet, the illuminated volumes were small enough to reduce crosstalk between medial and lateral stimulus locations (Fig. S10). Consistent with the hypothesis described above, we found the most prominent differences in the impact of optogenetic stimulation during whisker stimulation between medial crus 2 and lateral crus 1 (Figs. 4B and S11). More specifically, comparison of the impact of Purkinje cell stimulation on the extent of sensory-induced coherence revealed that Purkinje cells in medial crus 2 and lateral crus 1 differed in their impact on gamma band coherence, but showed no significant difference on theta band coherence. Since these data on regional heterogeneity were based on differential Purkinje cell modulations during different forms of adaptive and reflexive whisking behavior (28), they are consistent with the prominent dependency of the gamma, but not theta, band coherence on behavioral context (Fig. 3).

Dissecting the impact of neural pathways using a laminar model

We recapitulated the experimental findings by adapting a large-scale computational model of the laminar cortex and subcortical structures (16) to the anatomical pathways relevant for whisker and Purkinje cell stimulation (Fig. 5A). Increasing the intensity of Purkinje cell

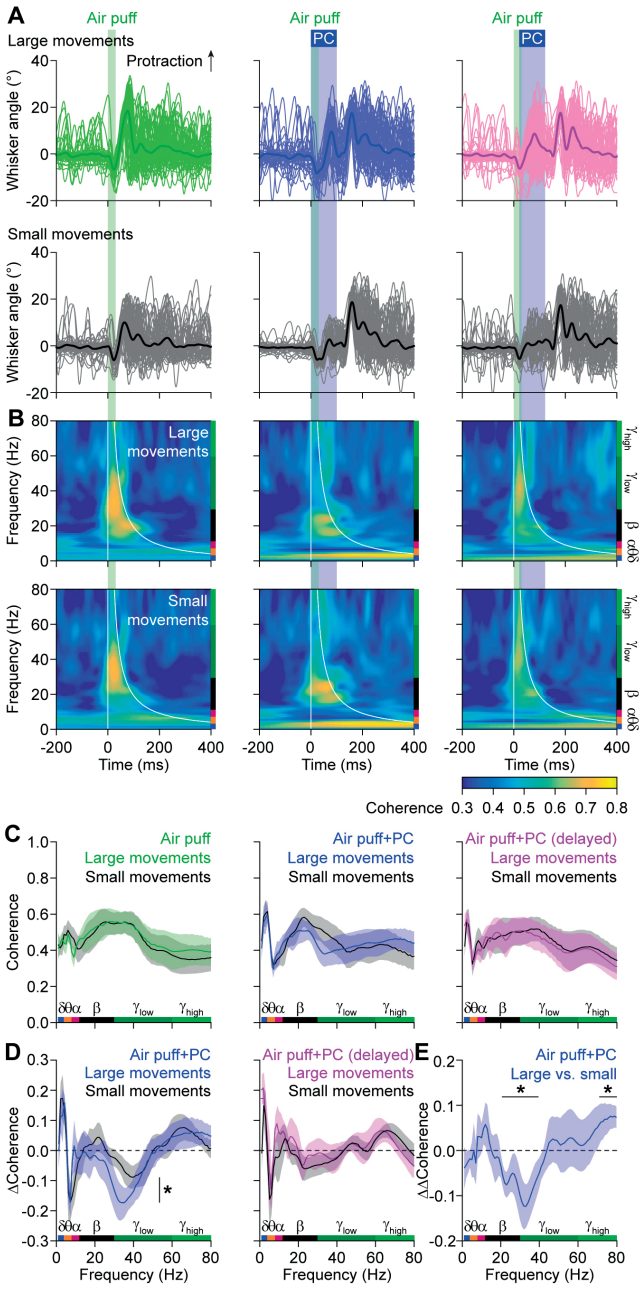

Figure 3. Cerebellar impact on wS1-wM1 coherence depends on behavior.

A Whisker stimulation triggers reflexive protraction. Trials were split between the 50% of the trials with the largest and the 50% with the smallest protractions. **B** The coherence between the subgranular layers of wS1 and the subgranular layers of wM1 were only mildly different between the trials with large (upper row) and small (bottom row) movements. **C** For each stimulus condition, the averaged coherence spectra are plotted, with colored traces representing the large whisker movements. Note that the difference in beta and lower gamma band activity are modulated in opposite fashion when adding optogenetic Purkinje cell stimulation to the air puff stimulation. **D** Accordingly, the impact of optogenetic Purkinje cell stimulation on sensory-induced wS1-wM1 coherence was stronger during trials with large whisker movements. This difference was statistically significant (DoC test, see **E**). This effect was abolished by a 20 ms delay between the start of whisker and Purkinje cell stimulation. **E** The difference in the impact of simultaneous Purkinje cell stimulation ("ΔΔCoherence") on sensory-induced beta and gamma band coherence was significantly larger during the trials with large movements than during those with small movements (DoC analysis). Lines in **C-E** indicate averages and the shades SEM. See also Fig. S7.

stimulation had differential effects on different regions, reflecting the contributions of excitatory and inhibitory connections between them (Fig. 5B). Stimulating the trigeminal nucleus, simulating whisker input, induced increased coherence in the theta and lower gamma range, the latter being inhibited by simultaneous Purkinje cell stimulation (Fig. 5C), mimicking the

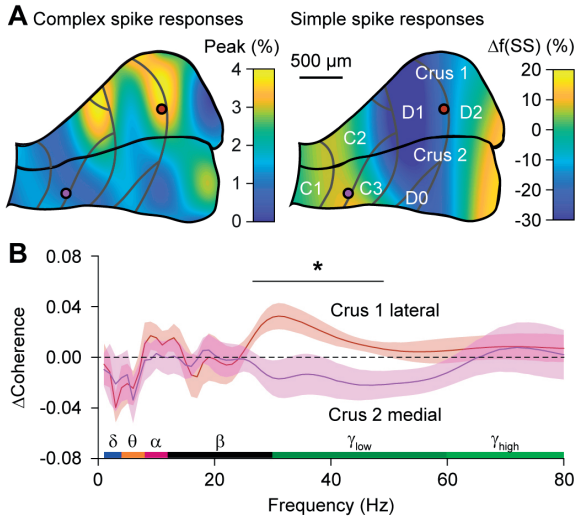

Figure 4. Regional heterogeneity in cerebello-cerebral communication.
A Air puff whisker pad stimulation results in bidirectional modulation of Purkinje cell simple spike firing. Heat map illustrates the distribution of the maximal modulation within 80 ms of stimulation, showing a difference between medial and lateral zones, modified with permission from (28). Note that whisker stimulation can either increase or decrease the simple spike rate. The grey lines indicate the tentative borders between the cerebellar zones. The two colored circles indicate the approximate positions of the 105 µm diameter optic fibers. **B** Compared to air puff stimulation in the absence of optogenetic stimulation, stimulation of Purkinje cells in the medial part of crus 2 and those in the lateral part of crus 1 had opposing effects specifically on sensory-induced gamma band coherence. See also Figs. S8-11.

experimental data (see Fig. 2). Granger causality analysis of the modeled data revealed that the sensory-induced gamma band coherence was approximately symmetrical between wS1 and wM1, while the theta band coherence caused by Purkinje cell activity was largely inflicted upon wS1 by wM1 (Fig. 5D). The balance between S1 and M1 in causing sensory-induced gamma band coherence proved to be particularly dependent on the reciprocal connectivity between the superficial layers of S1 and M1 (Fig. S12). Moreover, our model also fits with the results that Purkinje cell stimulation is responsible for the enhancement of theta coherence between cortical areas. Given the prominent similarity of the modeled and experimental datasets under various conditions, we next looked at the potential relevance of the different thalamic hubs that were not directly tested in the experiments. These modeling data suggest that the ventroposterior medial nucleus (VPM) and ventrolateral nucleus of the thalamus (VL) had a stronger impact than the medial posterior nucleus (Pom) in mediating the impact of cerebellar activation onto cortical coherence between wS1 and wM1 during sensory stimulation (Fig. S13), which is in line with the distribution of afferents from cerebellum and trigeminal nucleus to the thalamus (8).

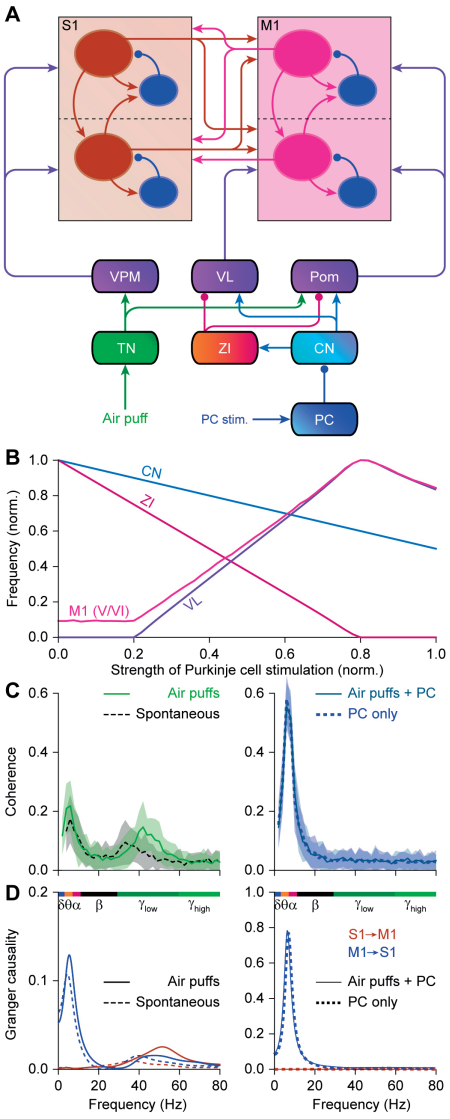

Figure 5. Laminar model.
A Schematic representation of the connections present in the computational model we used to study cortical coherence *in silico*. CN = cerebellar nuclei, PC = Purkinje cells, Pom = medial posterior nucleus of the thalamus, TN = sensory trigeminal nuclei, VL = ventrolateral nucleus of the thalamus, VPM = ventroposterior medial nucleus of the thalamus, ZI = zona incerta. **B** Impact of Purkinje cell stimulation on the firing rates of four different areas. **C** Coherence between S1 and M1 during stimulation of the trigeminal nuclei (simulating air puffs), the stimulation of Purkinje cells, and the combination of both stimuli. Trigeminal stimulation increased coherence in the gamma band, while Purkinje cell stimulation promoted theta band coherence. Adding Purkinje cell stimulation to trigeminal stimulation cancelled the increased gamma band coherence. Lines represent means and shaded areas sd. **D** Granger causality analysis revealing a largely bidirectional flow between S1 and M1 during gamma band coherence. Lower frequencies predominantly originated from M1. See also Figs. S12 and S13.

DISCUSSION

Tactile inspection of the world requires acute motor control with fast integration of sensory feedback. This is how one adapts grasp force to keep a slipping cup, or how a tennis player adapts his stroke to side wind. To study fast sensorimotor integration in mammals, exploration by whisker touch has become a popular model system (6-8). In line with the behavioral relevance to mice, neural control of the facial whiskers is complex, involving synergistic control of cerebellum and neocortex (23). Here, we found for the first time that transient disruptions of

cerebellar output, induced by optogenetic stimulation of Purkinje cells, could disinhibit sensory LFP responses to whisker stimulation in wS1 and wM1 and differentially modulate sensory-induced wS1-wM1 theta and gamma band oscillations. The impact of Purkinje cell stimulation on the coherence in the gamma, but not theta, range depended on the acute behavior as well as the precise location in the cerebellar cortex.

The impact of Purkinje cell stimulation on the individual LFP responses in wS1 and wM1 can be readily explained by the anatomical pathways involved (8). Whisker sensory information is rapidly relayed to the granular layer of wS1 via lemniscal and extralemniscal pathways passing by the thalamic VPM nucleus (8, 35-40). Optogenetic silencing of cerebellar output did not affect the initial excitation in the wS1 granular layer, but it did promote the subsequent spread to the subgranular layers (Fig. S4). These effects may be due to the prominent projection of the cerebellar nuclei onto the zona incerta (8, 38). Indeed, the inhibitory activity of the zona incerta has been implicated in subcortical suppression of whisker sensory input during self-motion (8, 37, 39, 40), which highlights its role as an important intermediate between cerebellum and neocortex. The zona incerta sends GABAergic projections in particular to Pom, which receives direct inputs from the trigeminal nuclei and cerebellum, next to its inputs from wS1 (8, 40) and VL (41). Thus, during whisker motion, the cerebellum could, in conjunction with wM1 (39), activate the zona incerta that in turn suppresses thalamic activity. In wS1, Pom terminals can be found mainly in layers I and V (42), in line with our finding of cerebellar disinhibition of the subgranular layers. In wM1 too, Purkinje cell stimulation resulted in a disinhibition of the sensory response, which again is compatible with the projections from Pom. Moreover, in all cases, a brief delay between sensory and Purkinje cell stimulation reduced the cerebellar impact substantially, which follows our experimental finding that a fast input from the cerebellum appears to be essential for the normal responses in wS1 and wM1.

The impact of Purkinje cell stimulation on coherence between wS1 and wM1 showed that cerebellar output enhances and reduces sensory-induced coherence in the theta and gamma bands, respectively. However, the finding that only the impact in the gamma range depended on ongoing behavior and on the precise location of stimulation in the cerebellar cortex raises the possibility that the cerebellum exerts its functional effects in the cortex mainly through a more high-frequency mode of operation. Moreover, these findings also suggest that the cerebellum may better control motor behavior by temporarily downgrading the coherence with sensory relevant signals rather than enhancing them. These implications agree with the high-frequency mode of simple spike activity and modulation that take place during the preparation and execution of motor coordination (28, 33, 43, 44). Indeed, we found that the suppressive impact of Purkinje cell stimulation on gamma band oscillations was greater during larger movements and this impact could be specifically linked to the Purkinje cells in medial crus 2. Finally, our data

also align well with the differential frequencies of coherences that are implicated during the different stages of motor planning and execution (9, 22).

The impact of cerebellar activation on individual LFP signals in wS1 or wM1 as well as that on the coherence between these signals could be well replicated by our modeling work. We built our computational model on cerebellar modulation of cortical interactions by expanding our existing model on cortico-cortical and thalamo-cortical interactions (16, 20). The model, the connectivity of which is constrained by realistic anatomical routes, suggests that Purkinje cell activity triggers a disinhibitory effect via the zona incerta, which in turn mediates both the suppression of gamma coherence and the enhancement of theta coherence between S1 and M1. In agreement with the experimental data, the model revealed that sensory-induced gamma band coherence involved mainly signals originating from S1, but with a substantial contribution of M1. The impact of M1 on gamma band coherence depended on the extent of reciprocal connectivity of S1 and M1, rather than on thalamic activity (Figs. S12). Changing the connectivity of the Pom could alter the coherence at lower frequencies, with the stronger connectivity being more in line with the experimental data, but had little impact on the directionality of coherence (Fig. S13). Given the similarities between the modeling and experimental outcomes, even explaining counterintuitive findings, the current model may well provide detailed and valid predictions as to how the cerebellum may influence the different layers and areas of the cerebral cortex under a wider and richer variety of physiological behaviors.

MATERIALS AND METHODS

Animals. Experiments were performed on heterozygous transgenic mice expressing the light-sensitive cation channel channelrhodopsin-2 under the Purkinje cell-specific *Pcp2* promoter (Tg(Pcp2-cre)2MPin;Gt(ROSA)26Sor$^{tm27.1(CAG-COP4*H134R/tdTomato)Hze}$) on a C57BL6/J background (45). We used 14 males and 12 females aged between 10 and 34 weeks. The mice were kept in a vivarium with controlled temperature and humidity and a 12/12 h light/dark cycle. The animals were group housed until surgery and single housed afterwards. A project license was obtained prior to the start of the experiments from the national authority (Centrale Commissie Dierproeven, The Hague, The Netherlands; license no. AVD101002015273) as required by Dutch law and all experiments were performed according to institutional, national and EU guidelines and legislation.

Surgery. The mice received a pedestal to allow head-fixation in the recording setup as well as one to three craniotomies to grant access to the brain. All surgical procedures were performed under anesthesia and the mice were given pain-killers before and after surgery. The animals were given three days of recovery after the surgery before they were habituated to the setup

on at least three consecutive days with increasing habituation times (from approx. 10 min the first session to approx. 2 h the last session). Further details can be found in the Supplementary Methods.

Electrophysiology. All recordings were made in awake, head restrained mice. Single unit activity of putative cerebellar nuclei neurons was measured using extracellular quartz-coated platinum-tungsten fiber electrodes (R = 2-5 MΩ; 80 µm outer diameter; Thomas Recording, Giessen, Germany) placed in a rectangular matrix (Thomas Recording) with an inter-electrode distance of 305 µm. LFP recordings were made in wS1 and wM1 using 16 channel, single shaft silicon probes with an inter-electrode distance of 100 µm (R = 1.5-2.5 MΩ, A1x16-5mm-100-177-A16, NeuroNexus Technologies, Ann Arbor, MI, USA). Each silicon probe was equipped with its own reference, placed in close proximity to the recording site. The two probes shared the same ground, which was placed either in the agar covering the recording sites or in the agar covering the cerebellar craniotomy. All electrodes were connected to a PZ5 NeuroDigitizer (Tucker-Davis Technologies). The signals were amplified, 1-6,000 Hz filtered, digitized at 24 kHz and stored using a RZ2 multi-channel workstation (Tucker-Davis Technologies). Recorded neurons were classified as putative cerebellar nuclei neurons if they were recorded at a depth of at least 1700 µm from the cerebellar surface and if the recording contained only a single type of action potentials typically showing both negative and positive parts, what differentiated them from Purkinje cell simple spikes. Spike times from single-unit recordings were retrieved off-line using Spiketrain (Neurasmus BV, Rotterdam, The Netherlands). Before any analysis was done on the LFP data, the raw traces were normalized using the z-score function in Matlab (MathWorks, Nattick, MA, USA). The current source density analysis was performed in custom written Matlab routines as detailed in the Supplementary Methods.

Coherence analysis. The phase coherence analysis was computed using the Fieldtrip toolbox as described in the Supplementary Methods. For this, LFP snippets of 5 second pre- and 5 second post-stimulus were used to calculate the coherence spectrum per trial. If necessary, 50 Hz line noise was removed. Next, the coherence in a 100 ms window after stimulus onset was averaged per frequency. The effect of Purkinje cell activation on the sensory triggered wS1-wM1 coherence was determined by subtracting the averaged air puff-induced coherence from the air puff with photostimulation evoked coherence. The Granger causality analysis was carried out by the Fieldtrip toolbox with the same preprocessing on the LFP data.

Stimulation. Optogenetic stimulation of the cerebellum occurred contralateral to the neocortical LFP recording sites using 470 nm LED drivers (M4703F, ThorLabs. Newton, NJ, USA) connected to a 4-channel LED driver (DC4104, ThorLabs) and optic fibers with diameters of 400 (Figs. 1-3) or 105 µm (Fig. 4) (ThorLabs). The 400 µm fibers were placed just above the dura of the cerebellum. The 105 µm fibers were adapted for insertion into the rectangular electrode

matrix by removing the cladding for ~15 cm and grinding the tip under microscope guidance. Unless stated otherwise, photostimulation was applied as 100 ms pulses with a power of 7.0 mW (400 µm fiber) or 0.2 mW (105 µm fiber). Sensory stimulations consisted of 30 ms air puffs at 1 bar directed at the mystacial macrovibrissae ipsilateral to cerebellar and contralateral to neocortical recording sites, using a MPPI-2 pressure injector (Applied Scientific Instrumentation, Eugene, OR, USA). The nozzle was positioned to minimize stimulation of the eye or ear. Stimuli were presented at 0.25 Hz in pseudorandom order.

Whisker movement tracking. Whisker movements in awake head-restrained mice were recorded with a high-speed video camera (frame rate 1,000 Hz; A504k camera, Basler, Ahrensburg, Germany), using a custom-made LED panel (λ = 640 nm) as back-light. All whiskers were kept intact. We tracked the whiskers as described previously (28, 46). For this study, the whisker position was defined as the average angle of all trackable whiskers. See the Supplementary Methods for more details.

Computational model. The computational model used is based on the one developed in (16), with (i) minimal variations in the cortical parameters based on the observed anatomical and physiological properties of wS1 and wM1 in mice and (ii) the addition of trigeminal nucleus, thalamic nuclei and cerebellar areas to the network.

Neocortex. Each cortical area is constituted by two cortical layers (or more generally, laminar modules) which describe the dynamics of superficial and deep layers, respectively. A laminar module contains one excitatory and one inhibitory population, and the dynamics of their respective firing rates $r_E(t)$ and $r_I(t)$ are described by the following equations:

$$\tau_E \frac{dr_E(t)}{dt} = -r_E t + F(I_E) + \sqrt{\tau_E}\,\sigma\,\xi(t)$$

$$\tau_I \frac{dr_I(t)}{dt} = -r_I t + F(I_I) + \sqrt{\tau_I}\,\sigma\,\xi(t)$$

Here, τ_E, τ_I denote the time scales for the excitatory and inhibitory populations respectively, and $\xi_E(t)$, $\xi_I(t)$ are Gaussian white noise terms of zero mean and standard deviation σ. For superficial layers, we choose $\tau_E = 6$ ms, $\tau_I = 15$ ms and $\sigma = 0.3$, which leads to a noisy oscillatory dynamics in the gamma range, and for deep layers we choose $\tau_E = 48$ ms, $\tau_I = 120$ ms and $\sigma = 0.45$, which leads to noisy oscillations in the theta and low alpha range. Note that the relatively high values for the time constants in deep layers are thought to reflect other slow biophysical factors not explicitly included in the model, such as the dynamics of NMDA receptors.

The function $F(x) = x/(1 - \exp(-x))$ is the input-output transfer function of each population, which transforms the incoming input currents into their corresponding cell-averaged firing

rates. The argument of the transfer function is the incoming current for each population, which involves a background term, a local term and a long-range term. The background term is a default constant current only received by excitatory neurons in S1 and M1, and it is $I_{bg} = 4$ for superficial excitatory neurons and $I_{bg} = 1$ for deep excitatory neurons. The local term involves the input coming from neurons within the area, and it is given by

$$I^{E}_{local} = 1.5\, r_E - 3.25\, r_I + I^{E}_{interlaminar}$$

$$I^{I}_{local} = 3.5\, r_E - 2.5\, r_I + I^{I}_{interlaminar}$$

Here, the numbers denote the strengths of the synaptic projections considered. The interlaminar terms are contributions from a different layer than the one the population is in. The only interlaminar projections are from superficial excitatory to deep excitatory neurons, with synaptic strength 1, and from deep excitatory to superficial inhibitory neurons, with synaptic strength 0.75 (24).

Finally, the long-range term includes currents coming from other neocortical or subcortical areas. These currents follow the general form $J_{ab}r_b$, (with J_{ab} being the synaptic strength from area 'b' to area 'a') and therefore we will specify only the synaptic coupling strengths to characterize them.

Following anatomical evidence (8), we consider excitatory projections from superficial S1 neurons to both superficial (strength 0.52) and deep (0.25) excitatory M1 neurons, and from deep S1 neurons to superficial (0.25) and deep (0.75) excitatory M1 neurons. In the opposite direction, we consider excitatory projections from superficial M1 neurons to both superficial (0.5) and deep (1) S1 excitatory neurons, and from deep M1 neurons to deep (1) S1 excitatory neurons.

The dynamics of the firing rate of the trigeminal nucleus (TN), the thalamic nuclei (VPM, VL and Pom) and cerebellar populations (PC, CN and ZI) are each described by equations of the type

$$\tau \frac{d\, r(t)}{dt} = -r(t) + f(I)$$

Here, $\tau = 10$ ms is the characteristic time constant and the transfer function is a threshold-linear function (i.e. $f(x) = Ax$, with A being the gain of the population, for $x>0$, and $f(x) = 0$ otherwise). The gain parameter A takes the values 3, 10, 1, 1, 0.5, 5 and 0.2 for areas TN, PC, CN, ZI, VPM, VL and Pom, respectively. Air puffs are modeled as a constant input (max I=10) to TN, while optogenetic stimulation to PC is modeled as a constant input (I=1). Cerebellar areas CN and ZI receive inhibitory projections (both of strength 1) from PC and CN respectively. In addition, PC

and CN received excitatory background currents of 0.1 and 21 respectively, and ZI receives an inhibitory background current of 12 (which can be also interpreted as a high firing threshold). Thalamic nuclei VPM received an excitatory projection (strength 1) from TN, VL receives projections from CN (strength 1) and ZI (strength -3), and Pom receives projections from TN (1), CN (0.2) and ZI (-0.5). Projections from VPM reach superficial excitatory (strength 0.66), deep excitatory (0.13) and inhibitory (0.2) populations of S1. Regarding M1, it receives projections from Pom to all its excitatory (0.33) and inhibitory (0.5) populations, and deep excitatory M1 neurons also receive a projection (0.6) from VL. When projections from Pom to S1 are considered (see Fig. S13), they target both excitatory (0.2) and inhibitory (0.15) populations in S1.

To mimic the depth of the recording electrodes for wS1 and wM1 in experiments, we estimate the LFP signal in the model by a weighted average of the excitatory superficial and deep layers, with a superficial:deep ratio of 1:9 for wS1 (i.e. deep layers) and 4:6 for wM1 (as it targets more superficial layers but it would still pick up signals from apical dendrites' layer V neurons).

Experimental design and statistical analysis. We considered $p \leq 0.05$ as significant unless Benjamini-Hochberg correction for multiple comparisons was applied (see Table S1). Two-tailed testing was used for all statistical analyses. *N* indicates the number of mice; *n* indicates the number of stimuli/recordings. Further details are in the Supplementary Methods.

ACKNOWLEDGMENTS

Financial support was provided by the Netherlands Organization for Scientific Research (NWO-ALW; CIDZ), the Dutch Organization for Medical Sciences (ZonMW; CIDZ), Life Sciences (CIDZ), ERC-adv and ERC-POC (CIDZ), as well as Crossover NWO-LSH INTENSE and Medical NeuroDelta. SH was supported by funding from the Okinawa Institute of Science and Technology Graduate University.

REFERENCES

1. P. Fries, Rhythms for Cognition: Communication through Coherence. *Neuron* **88**, 220-235 (2015).
2. A. K. Engel, P. König, A. K. Kreiter, T. B. Schillen, W. Singer, Temporal coding in the visual cortex: new vistas on integration in the nervous system. *Trends Neurosci* **15**, 218-226 (1992).
3. S. L. Bressler, R. Coppola, R. Nakamura, Episodic multiregional cortical coherence at multiple frequencies during visual task performance. *Nature* **366**, 153-156 (1993).
4. T. Womelsdorf, P. Fries, Neuronal coherence during selective attentional processing and sensory-motor integration. *J Physiol Paris* **100**, 182-193 (2006).
5. K. F. Ahrens, D. Kleinfeld, Current flow in vibrissa motor cortex can phase-lock with exploratory rhythmic whisking in rat. *J Neurophysiol* **92**, 1700-1707 (2004).
6. T. J. Prescott, M. E. Diamond, A. M. Wing, Active touch sensing. *Philos Trans R Soc Lond B Biol Sci* **366**, 2989-2995 (2011).
7. M. J. Z. Hartmann, A night in the life of a rat: vibrissal mechanics and tactile exploration. *Annals of the New York Academy of Sciences* **1225**, 110-118 (2011).
8. L. W. J. Bosman *et al.*, Anatomical pathways involved in generating and sensing rhythmic whisker movements. *Front Integr Neurosci* **5**, 53 (2011).
9. F. I. Arce-McShane, C. F. Ross, K. Takahashi, B. J. Sessle, N. G. Hatsopoulos, Primary motor and sensory cortical areas communicate via spatiotemporally coordinated networks at multiple frequencies. *Proc Natl Acad Sci U S A* **113**, 5083-5088 (2016).
10. T. van Kerkoerle *et al.*, Alpha and gamma oscillations characterize feedback and feedforward processing in monkey visual cortex. *Proc Natl Acad Sci U S A* **111**, 14332-14341 (2014).
11. H. Shin, C. I. Moore, Persistent gamma spiking in SI nonsensory fast spiking cells predicts perceptual success. *Neuron* 10.1016/j.neuron.2019.06.014 (2019).
12. J. Veit, R. Hakim, M. P. Jadi, T. J. Sejnowski, H. Adesnik, Cortical gamma band synchronization through somatostatin interneurons. *Nat Neurosci* **20**, 951-959 (2017).
13. J. A. Cardin et al., Driving fast-spiking cells induces gamma rhythm and controls sensory responses. *Nature* **459**, 663-667 (2009).
14. G. Buzsáki, X. J. Wang, Mechanisms of gamma oscillations. *Annu Rev Neurosci* **35**, 203-225 (2012).
15. O. Jensen, E. Spaak, J. M. Zumer, "Human brain oscillations: From physiological mechanisms to analysis and cognition" in Magnetoencephalography: From Signals to Dynamic Cortical Networks, S. Supek, C. J. Aine, Eds. (Springer Berlin Heidelberg, Berlin, Heidelberg, 2014), 10.1007/978-3-642-33045-2_17, pp. 359-403.
16. J. F. Mejias, J. D. Murray, H. Kennedy, X. J. Wang, Feedforward and feedback frequency-dependent interactions in a large-scale laminar network of the primate cortex. *Sci Adv* **2**, e1601335 (2016).
17. Y. B. Saalmann, M. A. Pinsk, L. Wang, X. Li, S. Kastner, The pulvinar regulates information transmission between cortical areas based on attention demands. *Science* **337**, 753-756 (2012).
18. W. Song, J. T. Francis, Gating of tactile information through gamma band during passive arm movement in awake primates. *Frontiers in neural circuits* **9**, 64 (2015).
19. C. Pedroarena, R. Llinás, Dendritic calcium conductances generate high-frequency oscillation in thalamocortical neurons. *Proc Natl Acad Sci U S A* **94**, 724-728 (1997).

20. J. Jaramillo, J. F. Mejias, X. J. Wang, Engagement of pulvino-cortical feedforward and feedback pathways in cognitive computations. *Neuron* **101**, 321-336 e329 (2019).
21. F. Vecchio et al., Acute cerebellar stroke and middle cerebral artery stroke exert distinctive modifications on functional cortical connectivity: A comparative study via EEG graph theory. *Clinical Neurophysiology* **130**, 997-1007 (2019).
22. D. Popa et al., Functional role of the cerebellum in gamma-band synchronization of the sensory and motor cortices. *J Neurosci* **33**, 6552-6556 (2013).
23. S. M. O'Connor, R. W. Berg, D. Kleinfeld, Coherent electrical activity between vibrissa sensory areas of cerebellum and neocortex is enhanced during free whisking. *J Neurophysiol* **87**, 2137-2148 (2002).
24. L. Kros et al., Cerebellar output controls generalized spike-and-wave discharge occurrence. *Ann Neurol* **77**, 1027-1049 (2015).
25. R. D. Proville et al., Cerebellum involvement in cortical sensorimotor circuits for the control of voluntary movements. *Nat Neurosci* **17**, 1233-1239 (2014).
26. C. I. De Zeeuw et al., Spatiotemporal firing patterns in the cerebellum. *Nat Rev Neurosci* **12**, 327-344 (2011).
27. U. Proske, S. C. Gandevia, The kinaesthetic senses. *J Physiol* **587**, 4139-4146 (2009).
28. V. Romano et al., Potentiation of cerebellar Purkinje cells facilitates whisker reflex adaptation through increased simple spike activity. *eLife* **7**, e38852 (2018).
29. C. P. J. De Kock, R. M. Bruno, H. Spors, B. Sakmann, Layer and cell type specific suprathreshold stimulus representation in primary somatosensory cortex. *J Physiol* **581**, 139 (2007).
30. I. Ferezou et al., Spatiotemporal dynamics of cortical sensorimotor integration in behaving mice. *Neuron* **56**, 907-923. (2007).
31. D. Kleinfeld, R. N. S. Sachdev, L. M. Merchant, M. R. Jarvis, F. F. Ebner, Adaptive filtering of vibrissa input in motor cortex of rat. *Neuron* **34**, 1021-1034 (2002).
32. L. W. J. Bosman et al., Encoding of whisker input by cerebellar Purkinje cells. *J Physiol* **588**, 3757-3783 (2010).
33. S. T. Brown, I. M. Raman, Sensorimotor integration and amplification of reflexive whisking by well-timed spiking in the cerebellar corticonuclear circuit. *Neuron* **99**, 564-575 (2018).
34. K. H. Pettersen, E. Hagen, G. T. Einevoll, Estimation of population firing rates and current source densities from laminar electrode recordings. *J Comput Neurosci* **24**, 291-313 (2008).
35. C. Yu, D. Derdikman, S. Haidarliu, E. Ahissar, Parallel thalamic pathways for whisking and touch signals in the rat. *PLoS Biol* **4**, e124 (2006).
36. T. Mao et al., Long-range neuronal circuits underlying the interaction between sensory and motor cortex. *Neuron* **72**, 111-123 (2011).
37. T. Furuta, N. Urbain, T. Kaneko, M. Deschênes, Corticofugal control of vibrissa-sensitive neurons in the interpolaris nucleus of the trigeminal complex. *J Neurosci* **30**, 1832-1838 (2010).
38. T. M. Teune, J. van der Burg, J. van der Moer, J. Voogd, T. J. Ruigrok, Topography of cerebellar nuclear projections to the brain stem in the rat. *Progress in brain research* **124**, 141-172 (2000).
39. N. Urbain, M. Deschênes, A new thalamic pathway of vibrissal information modulated by the motor cortex. *J Neurosci* **27**, 12407-12412 (2007).

40. C. B. Schäfer, F. E. Hoebeek, Convergence of primary sensory cortex and cerebellar nuclei pathways in the whisker system. *Neuroscience* **368**, 229-239 (2018).

41. P. Barthó, T. F. Freund, L. Acsády, Selective GABAergic innervation of thalamic nuclei from zona incerta. *Eur J Neurosci* **16**, 999-1014 (2002).

42. W. Zhang, R. M. Bruno, High-order thalamic inputs to primary somatosensory cortex are stronger and longer lasting than cortical inputs. *Elife* **8**, e44158 (2019).

43. Z. Gao et al., A cortico-cerebellar loop for motor planning. *Nature* **563**, 113-116 (2018).

44. F. P. Chabrol, A. Blot, T. D. Mrsic-Flogel, Cerebellar contribution to preparatory activity in motor neocortex. *Neuron* **103**, 506-519 e504 (2019).

45. L. Witter, C. B. Canto, T. M. Hoogland, J. R. de Gruijl, C. I. De Zeeuw, Strength and timing of motor responses mediated by rebound firing in the cerebellar nuclei after Purkinje cell activation. *Frontiers in neural circuits* **7**, 133 (2013).

46. N. Rahmati et al., Cerebellar potentiation and learning a whisker-based object localization task with a time response window. *J Neurosci* **34**, 1949-1962 (2014).

SUPPLEMENTARY METHODS

Surgery. All surgical procedures were performed under anesthesia (2-5% isoflurane in 1 l/min oxygen) in combination with treatment of surgical pain giving 5 mg/kg carprofen ("Rimadyl", Pfizer, New York, NY, USA), 1 µg bupivacaine (Actavis, Parsippany-Troy Hills, NJ, USA) and 50 µg/kg buprenorphine ("Temgesic", Indivior, Richmond, VA, USA). In addition, the mice received 1 µg lidocaine (Braun, Meisingen, Germany) subcutaneously at the surgical sites prior to the start of the surgery. The body temperature was maintained at 37 °C by a feed-back controlled heating pad.

For the placement of a pedestal, a part of the skin was removed and the skull was cleaned and treated with phosphoric acid to ensure all membranes were removed. Next, the exposed skull was treated with Optibond adhesive (Kerr Dental, Orange, CA, USA) and the mice received a magnetic pedestal that was placed on the skull between the eyes and secured with Charisma (Kerr Dental). Next, up to three craniotomies were performed allowing access to the whisker part of the left primary somatosensory (wS1, relative to bregma: 3.5 mm mediolateral and -1.5 mm anteroposterior) and motor cortex (wM1, relative to bregma: 1.5 mm mediolateral and 1.0 mm anteroposterior) and the right cerebellar hemisphere, each surrounded by a recording chamber made out of Charisma. The exposed dura was covered with tetracycline-containing ointment (Terra Cortril; Pfizer, New York, NY, USA) and the recording chambers were sealed with a silicon polymer (Kwik-Cast, WPI, Sarasota, FL, USA) and covered with bone wax (Ethicon, Somerville, NJ, USA). The animals were given three days of recovery after the surgery before they were habituated to the setup on at least three consecutive days with increasing habituation times (from approx. 10 min the first session to approx. 2 h the last session).

Electrophysiology. Local field potentials (LFP) were recorded in wS1 and wM1 using linear silicon probes. Each silicon probe was equipped with its own reference, placed in close proximity to the recording site. The two probes shared the same ground, which was placed either in the agar covering the recording sites or in the agar covering the cerebellar craniotomy. The platinum-tungsten electrodes as well as the silicon probes were connected to a PZ5 NeuroDigitizer (Tucker-Davis Technologies (TDT), Alachua, FL, USA). The signals were amplified, 1-6,000 Hz filtered, digitized at 24 kHz and stored using a RZ2 multi-channel workstation (TDT).

Before any analysis was done on the LFP data, the raw traces were normalized using the z-score function in MATLAB (MathWorks, Nattick, MA, USA). The current source density analysis was performed in custom written MATLAB routines using the Kernel Source Density Method as described in (1); see https://github.molgen.mpg.de/MPIBR-coattia/MatlabMain/tree/master/behaviorAnalysis/code/functions/kCSDv1.

In the cerebellum, recorded neurons were classified as originating from putative cerebellar nuclei neurons if they were recorded at a depth of at least 1700 µm from the cerebellar surface and if the recording contained only a single type of action potentials, what differentiated them from Purkinje cell recordings. Spike times were retrieved off-line using SpikeTrain (Neurasmus

BV, Rotterdam, The Netherlands). After automated spike detection and sorting, all traces were inspected manually and improper event classification was corrected.

Coherence analysis. The phase coherence analysis was computed using the Fieldtrip toolbox (2). For this, LFP snippets of 5 second pre- and 5 second post-stimulus were used to calculate the coherence spectrum per trial. If necessary, line noise at 50 Hz was removed first from the waveforms by fitting a PSD around the time of the peaks of the power spectrum and then filtering the signal with the inversed square root of this function. Next, the coherence in a frequency-dependent window (2 * 1/frequency) after stimulus onset was averaged per frequency to perform the further analysis on. The effect of optogenetic Purkinje cell activation on the sensory triggered wS1-wM1 coherence was determined by subtracting the averaged air puff induced coherence from the air puff with optogenetically evoked coherence. To test for differences between the conditions, the difference of coherence test was used, as described by Amjad et al. (3). In short, the Fisher transform ($\tanh^{-1}$) was applied on the coherence and this was compared to a χ^2-distribution with $k - 1$ degrees of freedom, where k is the number of conditions that were tested (in all cases $k = 2$). The 95% confidence limit was then determined using $\chi^2_{(0.05;1)} = 3.84$. The significant frequencies are indicated in the difference of coherence figures using lines and asterisks.

Whisking behavior. Whisker movements were tracked off-line using the BIOTACT Whisker Tracking Tool (BWTT) with the sdGeneric, stShapeSpaceKalman, ppBigExtractionAndFiltering, and wdIgorMeanAngle plugins (http://bwtt.sourceforge.net) (4). Briefly, we first determined

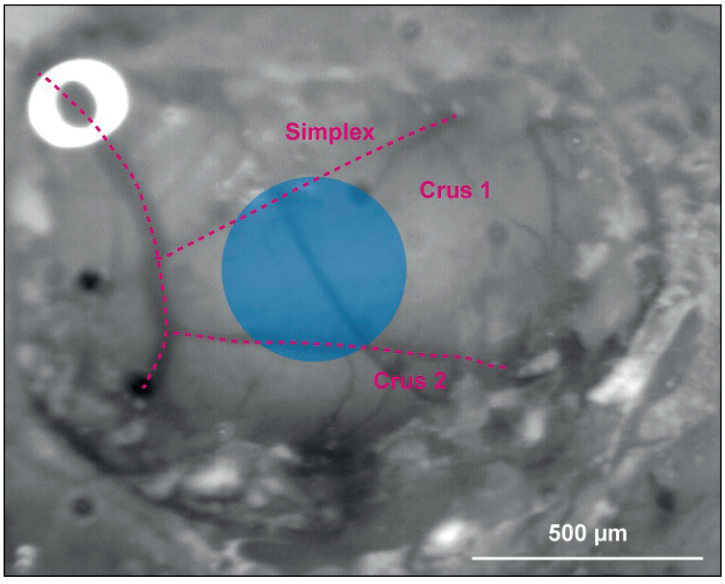

Figure S1. Location of optogenetic stimulation.
Approximate location of a 400 µm diameter optic fiber in the center of crus 1 as seen through the craniotomy.

the position of the snout in each frame semi-automatically by fitting a template to the snout. After masking the snout and subtracting the unmoved background from each frame, the whiskers were traced in a radial approach. The algorithm detected edges in the frame in consecutive concentric snout-shaped masks around the actual snout mask. Ultimately, we detected the start and end nodes of the fitted line segments, and calculated the angles of the whiskers from these values. The final BWTT result provided us with the angles of all detected whiskers per video frame. To relate the angles across frames to the tracks, we wrote an algorithm that predicts track values in consecutive frames based on the position and velocity in the angular value as well as the y-position of the last video frames (5, 6). The predicted track values for the next frame were compared with the detected values in the next frame and were assigned according to a minimum deviation approach between them. Finally, the mean angle per frame was calculated from the individual whisker traces.

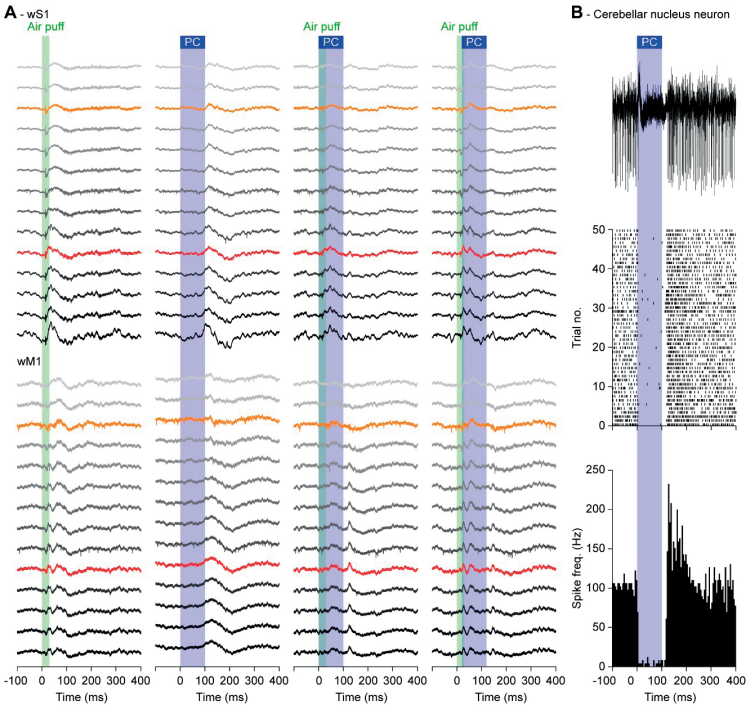

Figure S2. Purkinje cell stimulation reduces the impact of whisker stimulation on wS1 and wM1.
A Air puff stimulation of the large facial whiskers evoked sensory responses in contralateral wS1 and wM1, recorded here as deviations in the local field potential (LFP) of a randomly selected single trial (left column). The LFP recordings were made using linear silicon probes with 100 µm inter-electrode distances. The recordings are organized from superficial to deep (color code as in Fig. 1B). Electrodes 3 and 10, that were used for most analyses in this study, are marked with orange and red, respectively. Optogenetic stimulation of Purkinje cells (PC) was done with an optic fiber with a diameter of 400 µm placed on the center of crus 1 (see Fig. S1), leading to a delayed response in both wS1 and wM1 (2nd column). The other columns depict randomly selected trials from the same experiment, showing respectively the combined sensory and optogenetic Purkinje cell stimulation and the latter with a delay of 20 ms before the onset of the Purkinje cell stimulation. **B** Optogenetic Purkinje cell stimulation leads to a pause in firing of an exemplary neuron in the cerebellar nuclei, followed by rebound firing after the end of stimulation. Further analysis of cerebellar nuclear activity is presented in Figs. S8-S10.

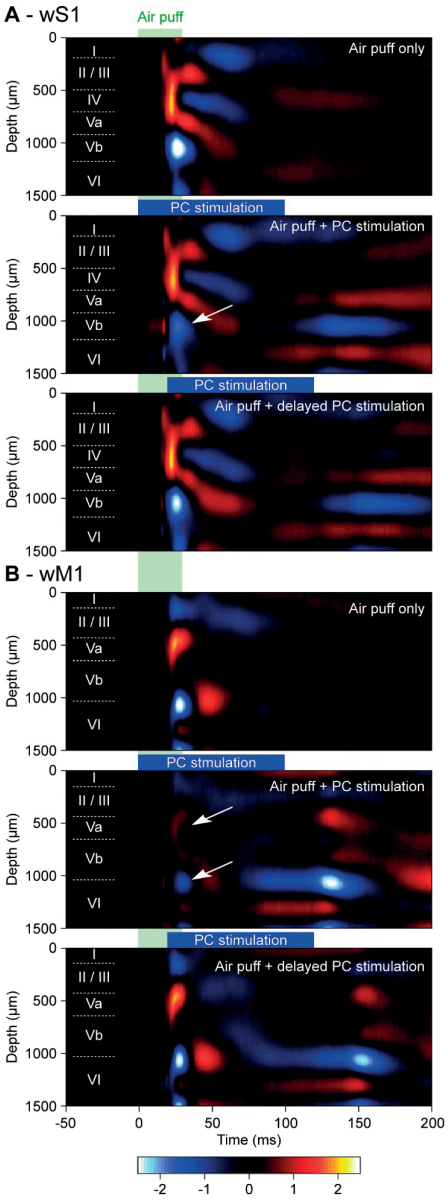

Figure S3. Purkinje cell stimulation reduces sensory responses in wS1 and wM1.

A Current source density analysis of the averaged local field potentials across the layers of the whisker area of S1 (see Fig. 1C-H) during whisker air puff stimulation alone or in combination with optogenetic stimulation of Purkinje cells using an optic fiber with a diameter of 400 µm placed on the center of crus 1 (see Fig. S1). Purkinje cell stimulation applied simultaneously with whisker stimulation suppressed predominantly the fast current sinks (blue; white arrow), but a 20 ms delay between air puff and whisker stimulation largely restores the impact of air puff stimulation. **B** The same was true for the whisker area of wM1. The heat maps indicate the averaged values of 8 mice with color scaling in arbitrary units. The layers of wS1 and wM1 are indicated by approximation.

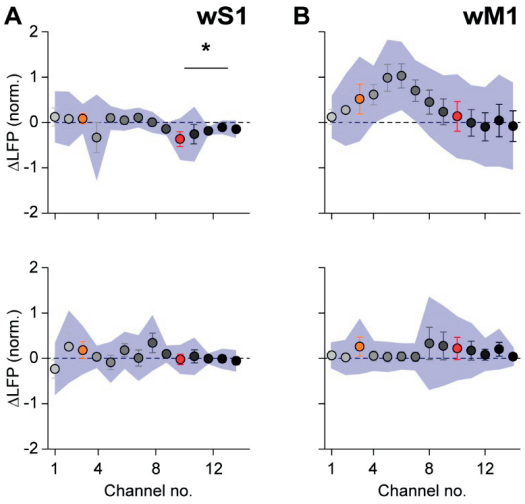

Figure S4. Optogenetic Purkinje cell stimulation increases the spread of excitation triggered by whisker stimulation.

A Air puff whisker stimulation triggers excitation in contralateral wS1 and wM1. In wS1, the amplitude of the first negative LFP peak (corresponding to excitatory activity) in the subgranular layers was enhanced ($p = 0.012$, $\chi^2 = 2.500$, Dunn's post-hoc test after Friedmann's ANOVA, Table S1). This effect was absent upon introducing a delay of 20 ms between whisker and Purkinje cell stimulation (bottom row). **B** The same for wM1. Plotted are the averaged differences in amplitude of the first positive LFP peaks. Error bars indicate SEM and shaded area sd. $n = 100$ trials each in $N = 8$ mice.

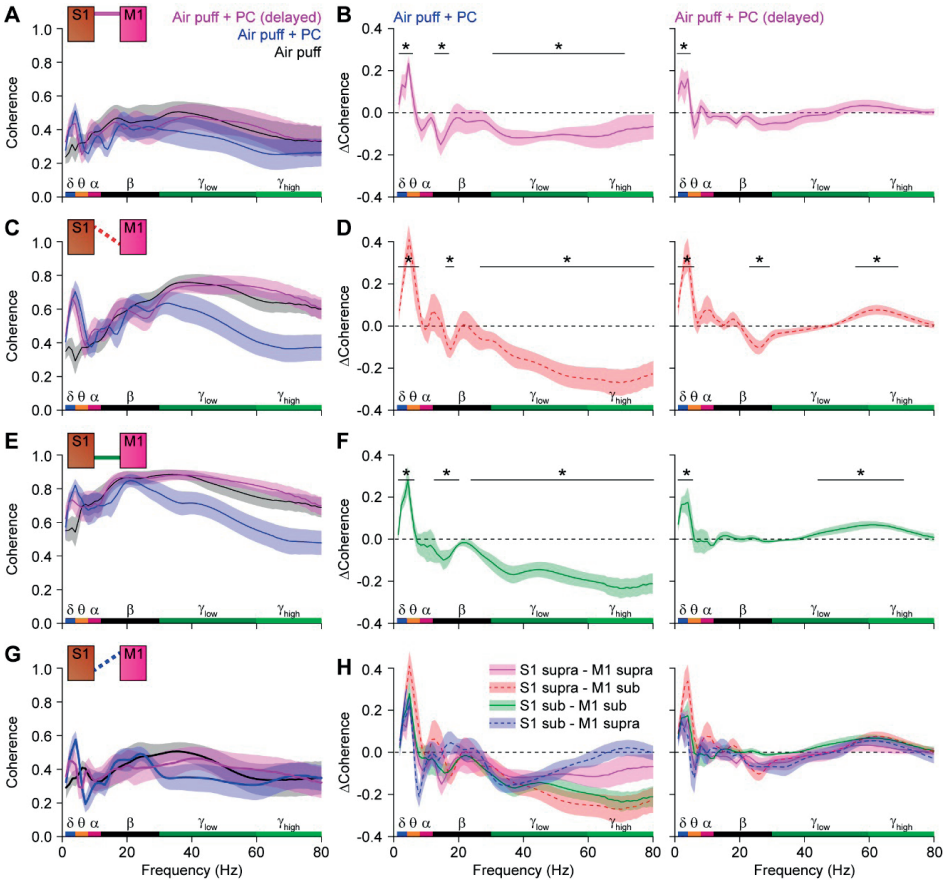

Figure S5. Cerebellar Purkinje cell stimulation suppresses sensory-induced gamma band coherence between wS1 and wM1.

A Averaged coherence between the supragranular layers of wS1 and wM1 following air puff stimulation of the contralateral facial whiskers in isolation or in combination with simultaneous or 20 ms delayed optogenetic stimulation of Purkinje cells using an optic fiber with a diameter of 400 µm placed on the center of crus 1 (see Fig. S1). Shaded areas indicate SEM. $n = 100$ trials per condition each in $N = 8$ mice. **B** Purkinje cell stimulation suppressed mainly the gamma band coherence induced by air puff sensory stimulation. This effect was largely abolished by introducing a 20 ms delay between the start of the sensory stimulation and that of the Purkinje cells. **C-H** The same for the coherence between different layers of wS1 and wM1 as indicated schematically in the upper left corners. Although the details varied to some extent, in all cases Purkinje cell stimulation suppressed sensory-induced gamma band coherence between wS1 and wM1. * $p < 0.05$ ($\chi^2 > 3.84$; difference of coherence test, see Methods).

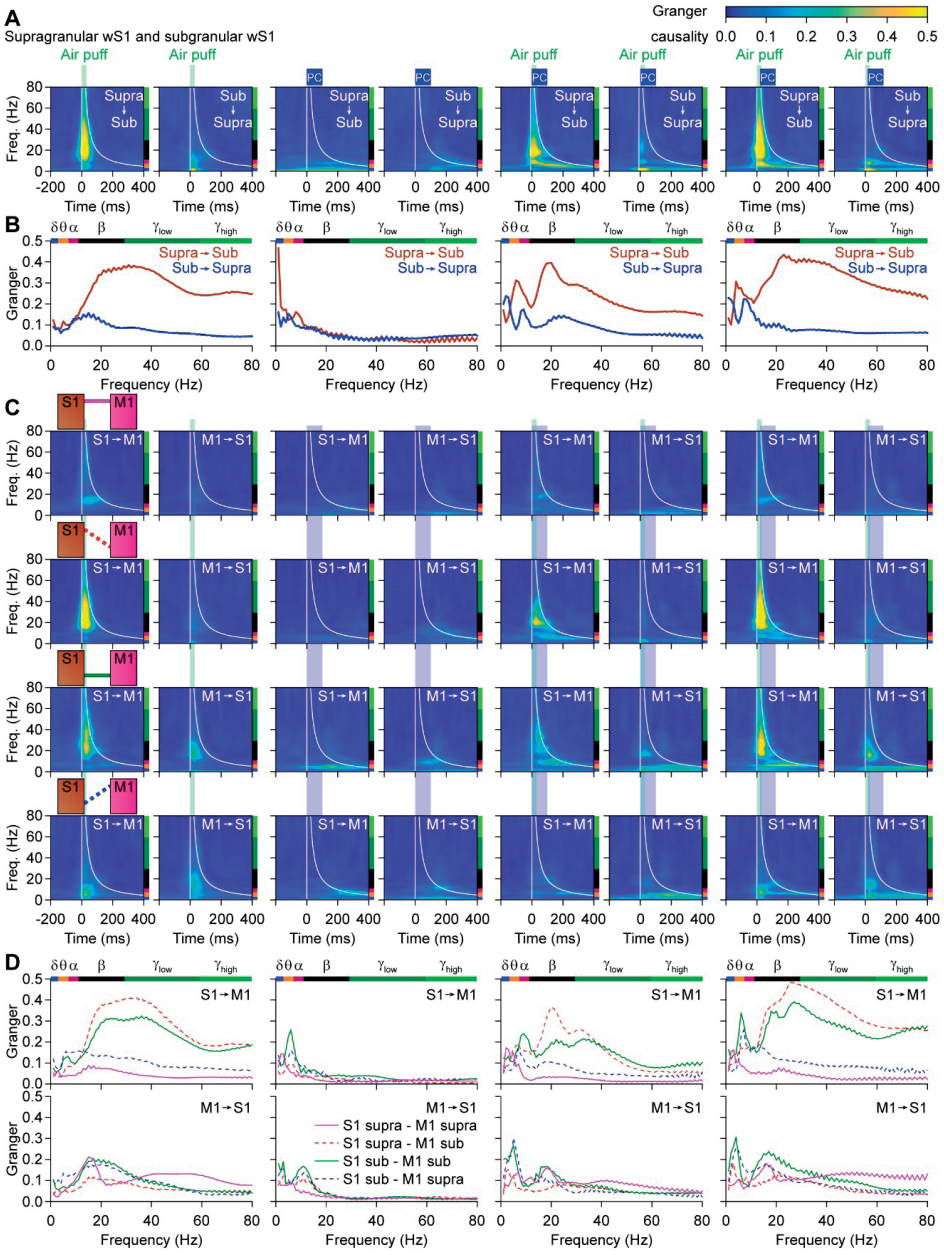

Figure S6. Granger causality analysis.

A Granger causality analysis revealed that the sensory-induced beta and gamma band coherence within wS1 was mainly caused by activity in the supragranular layers. The flow from the superficial to the deeper layers in the gamma, but not the beta, band was disrupted by simultaneous Purkinje cell stimulation. **B** The mean Granger causality values for the different conditions, comparing the flow from superficial to deep layers vs. the flow from deep to superficial layers. **C** Granger causality analysis of the coherence between wS1 and wM1, expanding on the analysis shown in Fig. 2C-D where the subgranular layers of wS1 were compared to the supragranular layers of wM1 (data copied in the fourth row to facilitate comparisons). This analysis suggest that the sensory-induced gamma band coherence is mainly caused by the superficial layers of wS1, and

from there spreads over wS1 and wM1. The strongest interconnections are found between subgranular layers of wS1 and the supragranular layers of wM1 (fourth row). Also here, wS1 drives wM1 stronger than vice versa, but also wM1 has a share in this coherence, stressing the importance of the connections between wS1 and wM1. **D** The mean Granger causality values for the different relations between wS1 and wM1.

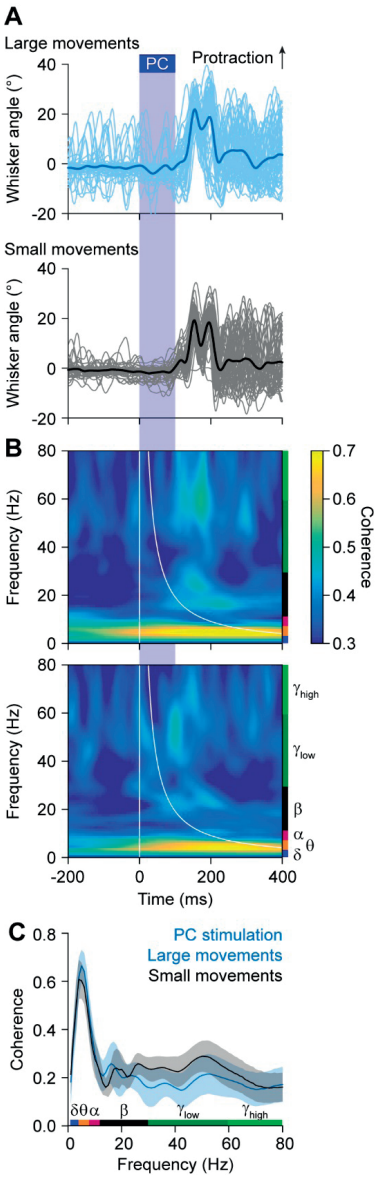

Figure S7. Optogenetic Purkinje cell stimulation induces delayed whisker protraction.
A Optogenetic stimulation of Purkinje cells, using a 400 µm diameter optic fiber placed on the center of crus 1, induced whisker protraction at the end of the stimulus. Shown are the 100 trials of a representative experiment, split into the 50% of the trials with the largest and the 50% with the smallest protraction. **B** Heat maps of the coherence over time, showing predominantly activity in the theta band, that was not different between the groups of trials (**C**). *N* = 8 mice. Shades indicate SEM.

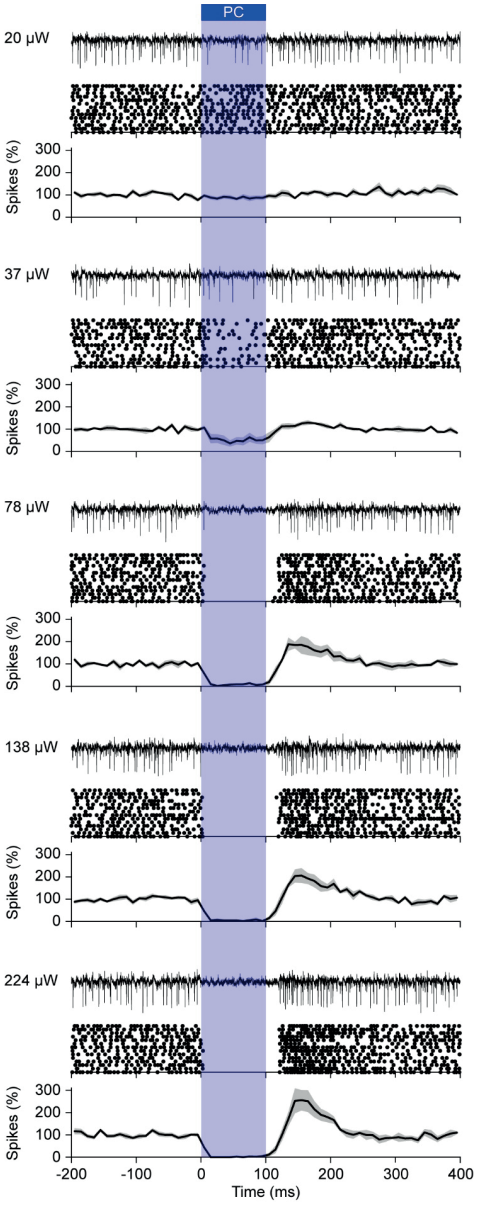

Figure S8. Optogenetic stimulation of Purkinje cells silences neurons of the cerebellar nuclei.
Using different illumination intensities and an optic fiber with a diameter of 105 µm, optogenetic stimulation of Purkinje cells induced a pause in firing of cerebellar nuclei neurons. At higher intensities, the pause was followed by rebound firing. For each intensity, an example trace is plotted, followed by a raster plot of the same experiment and the averaged peri-stimulus histogram of the spike rate (normalized to baseline = 100%) constructed from 6 responsive neurons in *N* = 2 mice. The shades indicate SEM.

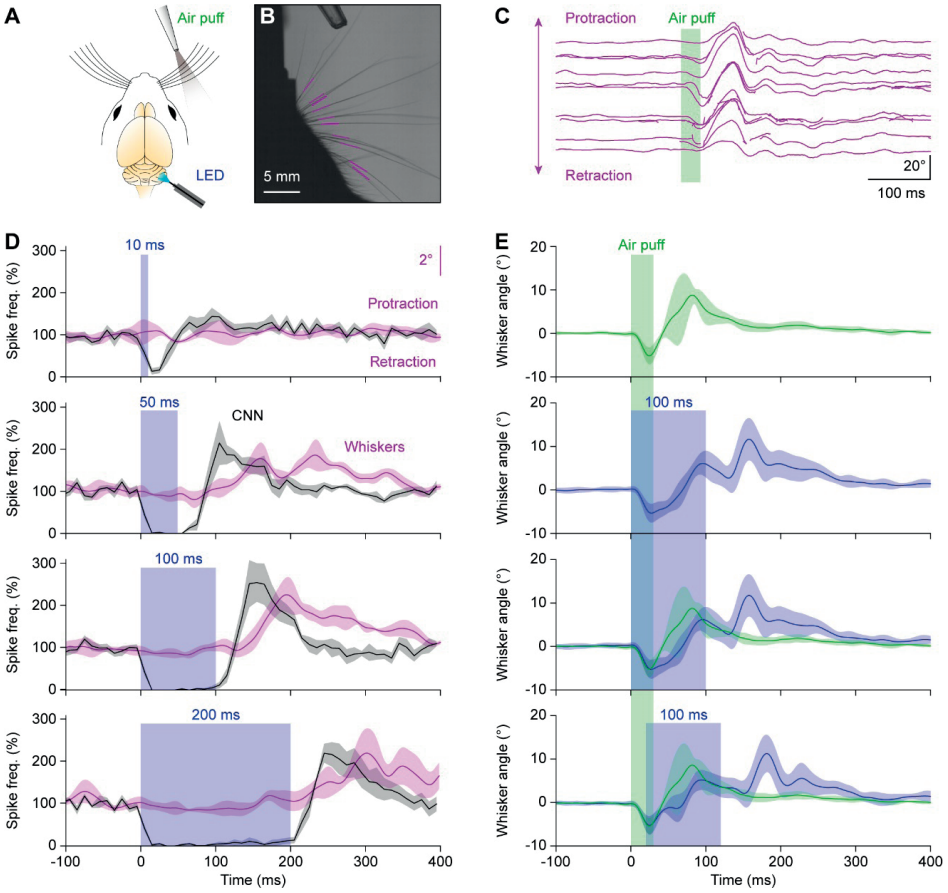

Figure S9. Rebound firing in the cerebellar nuclei is linked to whisker protraction.

A Experimental scheme. **B** The movements of the whiskers were tracked using video-analysis. The colored line fragments indicate the tracked part of the whiskers. **C** Raw output of the whisker tracking algorithm, showing for one trial how an air puff blew the whiskers backwards, after which an active protraction followed. **D** Optogenetic stimulation could also trigger whisker protraction, but not during the period of stimulation. By varying the stimulus duration, we observed that the rebound firing in the cerebellar nucleus neurons (CNN) varied in timing and amplitude and that the whisker protraction followed the rebound firing. *n* = 6 cerebellar nucleus neurons in *N* = 2 mice. E Whisker air puff stimulation induced a reflexive protraction. This protraction was reduced during the stimulus, but increased at the end of the stimulus. The whisker angle was normalized for each mouse at 0° before stimulus onset. *N* = 4 mice with each *n* = 100 trials per condition. Lines indicate average and shades SEM.

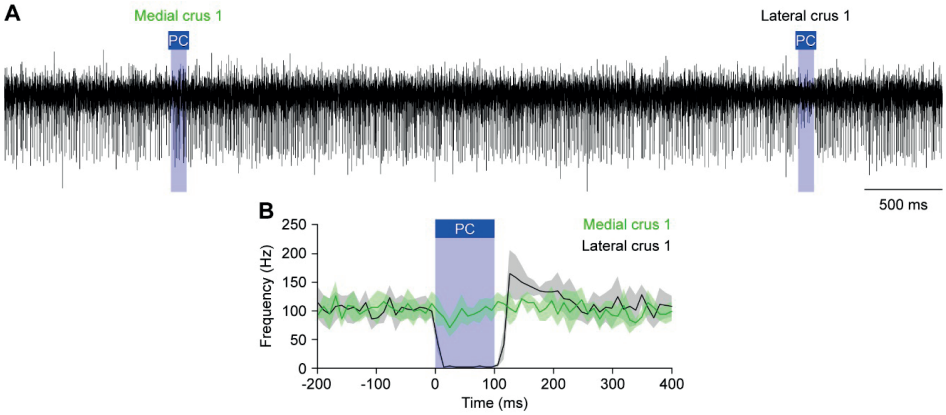

Figure S10. Optogenetic Purkinje cell stimulation acts locally.
A Extracellular recording of an exemplary cerebellar nucleus neuron displaying inhibition upon optogenetic stimulation of Purkinje cells in the lateral, but not the medial part of crus 1. For this experiment, an optic fiber with a diameter of 105 µm was used. **B** Averaged peri-stimulus histogram of two simultaneously recorded cerebellar nucleus neurons. The two neurons were separated laterally by 305 µm.

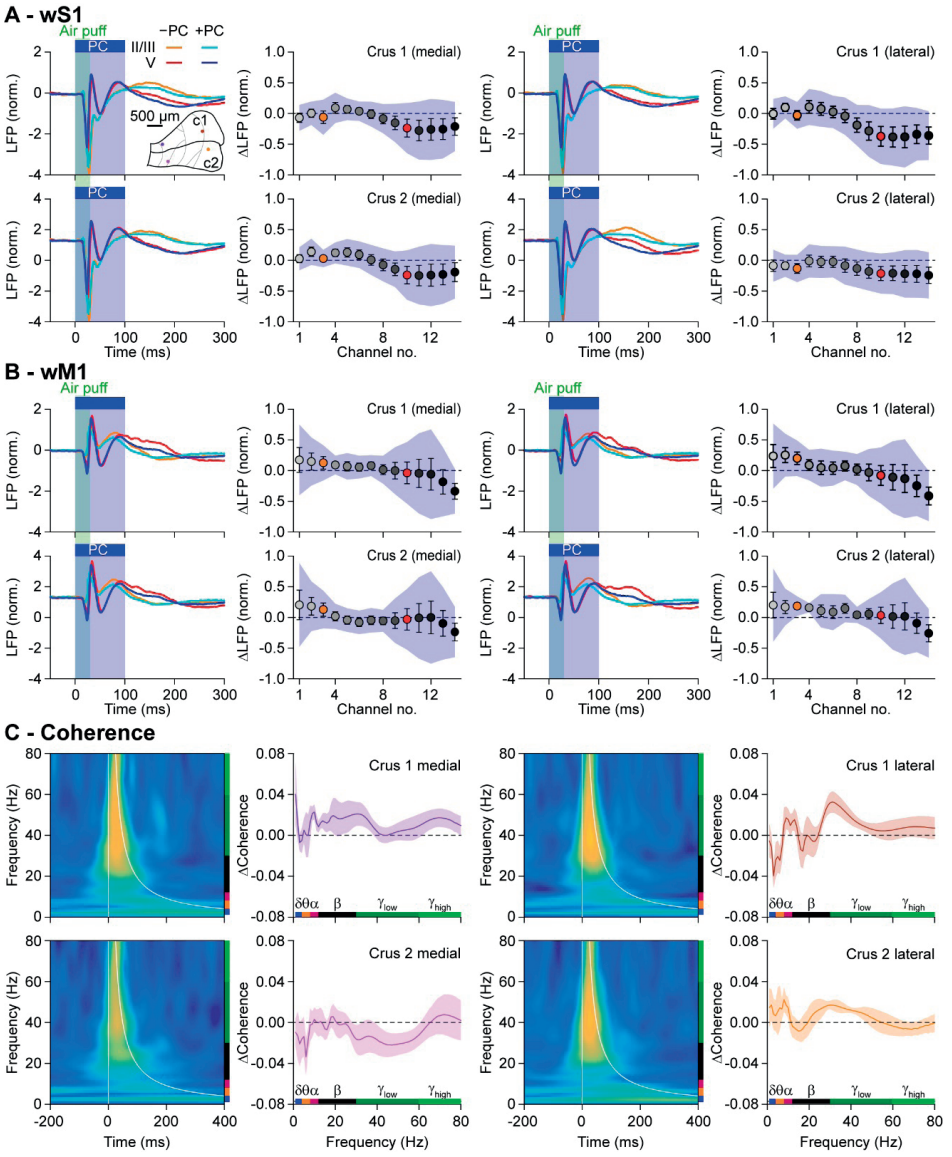

Figure S11. Regional differences in the impact of Purkinje cell stimulation on sensory-induced local field potentials in wS1 and wM1.

A Averaged local field potentials (LFP) of the supra- (light colors) and subgranular (dark colors) of wS1 upon either only air puff stimulation of the contralateral facial whiskers (red colors) or air puff stimulation in combination with optogenetic stimulation of Purkinje cells (PC; blue colors). Optogenetic Purkinje cell stimulation was performed using four optic fibers with 105 µm diameter placed at different locations in crus 1 (c1) and crus 2 (c2; inset). During each trial, one of the fibers was activated in a random sequence. The 2nd and 4th columns indicate the difference in the amplitudes of the first positive peaks following stimulation, using the same color codes as in Fig. 1. Error bars indicate SEM and shaded areas sd. **B** The same analysis, but now for wM1. **C** Combined air puff whisker stimulation and optogenetic Purkinje cell stimulation resulted in gamma band coherence between wS1 and wM1 (heat maps). The coherence was different from those trials in which only the whiskers were stimulated, as indicated by the ΔCoherence plots. The impact of Purkinje cell stimulation on sensory-induced coherence depended on the location of optogenetic stimulation, with the lateral part of crus 1 and the medial part of crus 2 having op-

posite impact on gamma (but not theta) band coherence and the other locations having more intermediate effects. Lines are averages and shaded areas indicate SEM. *N* = 7 mice.

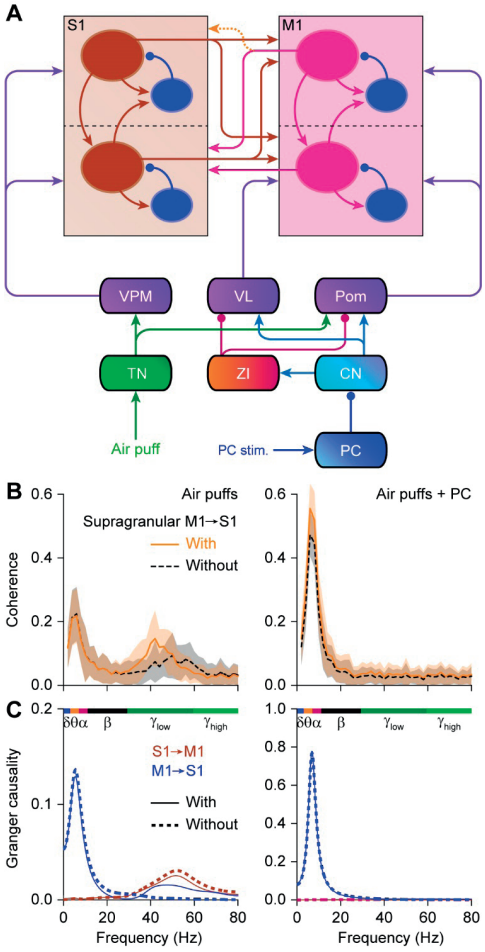

Figure S12. Laminar model: impact of a projection for the supragranular layers of M1 to the supragranular layers of S1.

A Here we compared the circuit with and without a direct connection between the supragranular layers of M1 and S1 (dashed orange arrow). **B** Removing the supragranular M1 to S1 connection resulted in a slightly less powerful gamma band coherence (black) upon simulation of the trigeminal nuclei (simulating sensory input of the whiskers) than the same simulation in the presence of the supragranular M1 to S1 connection (orange). The impact of this connection was less during the combined trigeminal + Purkinje cell stimulation. C Granger causality analysis revealed that deleting the supragranular M1 to S1 connection resulted in a virtually complete lack of the contribution of M1 to the sensory-induced gamma band coherence. Note that the situation with the supragranular M1 to S1 connection is the circuit that was used to generate the data of Fig. 5. These data are replicated here to facilitate comparison. Lines indicate averages and shaded areas sd.

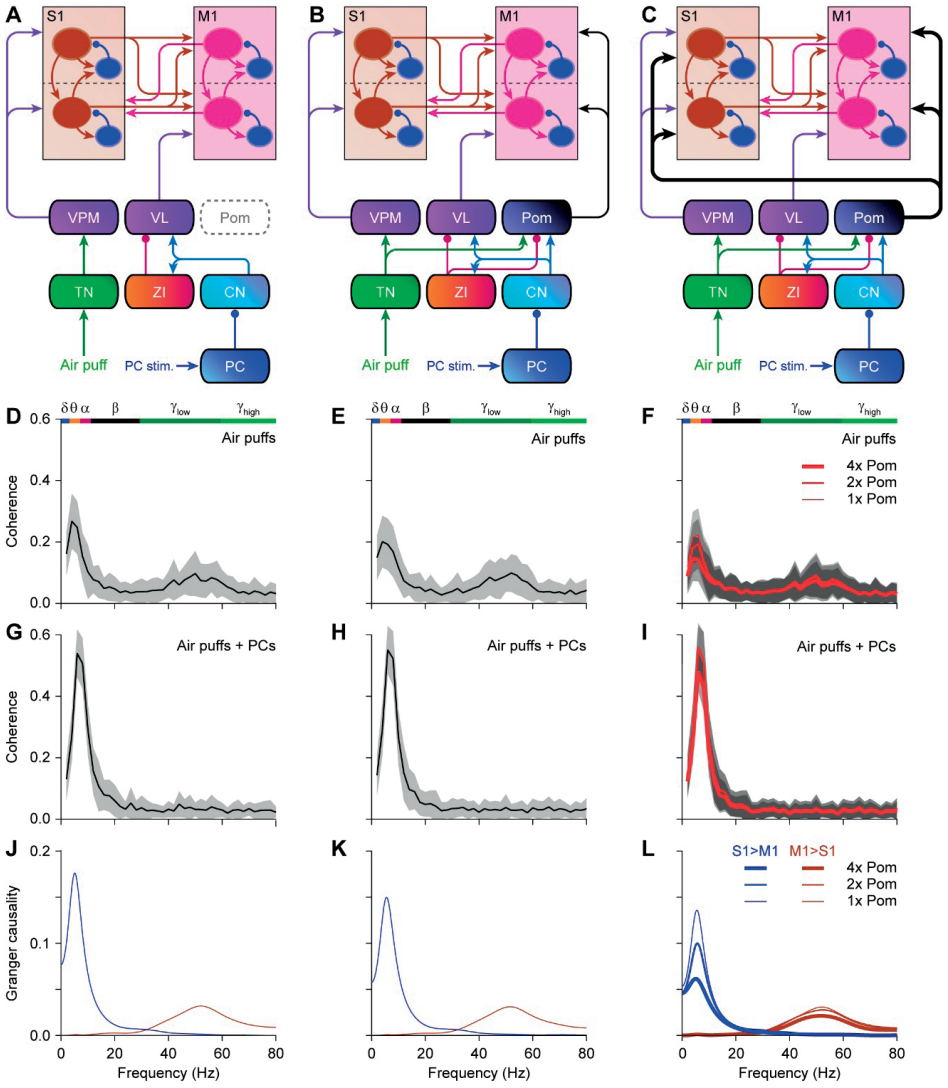

Figure S13. Impact of Pom connectivity on laminar model

To test whether the Pom could affect the flow between S1 and M1 during gamma band coherence, we used our computation model in the configuration without a supragranular connection between M1 and S1 (Fig. S12). In this configuration, S1 is dominant over M1 when generating gamma band coherence. To study the impact of the Pom, we compared three different configurations: without Pom (**A**), with Pom projecting only to M1 (**B**) and with Pom symmetrically projecting to S1 and M1 (**C**). Of the latter, we implemented the connectiivty strength as used for Pom to M1 connection in Fig. 5, double ("2x Pom") and quadruple strength ("4x Pom). **D-F** The different configurations did affect the amplitude of sensory-induced coherence between S1 and M1 (simulated by stimulation of the trigeminal nuclei), but did not affect the frequency characteristics. **G-I** A similar observation was made for the conjunctive trigeminal + Purkinje cell stimulation. **J-L** Granger causality analysis demonstrated that the Pom could not induce M1 to be causative for sensory-induced gamma band coherence (as the direct supragranular connection between M1 and S1 could; see Fig. S12). Lines indicate averages and shaded areas sd.

Table S1.

	p	χ^2	Sign.?	Test
First negative peak				
wS1 [supragranular layers]	0.417	1.750		Friedman's
wS1 [layer IV]	0.197	3.250		Friedman's
wS1 [subgranular layers]	**0.030**	7.000		Friedman's
Air puff vs. Air puff + simultaneous PC stimulation	***0.012***	*2.500*	*yes*	*Dunn's*
Air puff vs. Air puff + delayed PC stimulation	*0.046*	*-2.000*	*no*	*Dunn's*
Simultaneous vs. delayed stimulation	*0.617*	*0.500*	*no*	*Dunn's*
wM1 [supragranular layers]	0.093	4.750		Friedman's
wM1 [subgranular layers]	0.417	1.750		Friedman's
First positive peak				
wS1 [supragranular layers]	0.607	1.000		Friedman's
wS1 [layer IV]	0.325	2.250		Friedman's
wS1 [subgranular layers]	**0.008**	9.750		Friedman's
Air puff vs. Air puff + simultaneous PC stimulation	***0.024***	*2.250*	*yes*	*Dunn's*
Air puff vs. Air puff + delayed PC stimulation	*0.453*	*-3.000*	*no*	*Dunn's*
Simultaneous vs. delayed stimulation	***0.003***	*-0.750*	*yes*	*Dunn's*
wM1 [subgranular layers]	**0.030**	7.000		Friedman's
Air puff vs. Air puff + simultaneous PC stimulation	0.617	-0.500	*no*	*Dunn's*
Air puff vs. Air puff + delayed PC stimulation	**0.012**	-2.500	*yes*	*Dunn's*
Simultaneous vs. delayed stimulation	0.046	-2.000	*no*	*Dunn's*
wM1 [subgranular layers]	0.008	9.750		Friedman's
Air puff vs. Air puff + simultaneous PC stimulation	***0.024***	*2.250*	*no*	*Dunn's*
Air puff vs. Air puff + delayed PC stimulation	*0.453*	*-3.000*	*yes*	*Dunn's*
Simultaneous vs. delayed stimulation	***0.003***	*-0.750*	yes	*Dunn's*

Statistical evaluation of the data represented in Figs. 1 and S4. For each mouse, the averages of the first negative and the first positive peak were compared between three conditions (only air puff stimulation of the whiskers, simultaneous air puff and optogenetic Purkinje cell (PC) stimulation and air puff stimulation combined with a 20 ms delayed PC stimulation. Averages were compared with Friedman's two-way ANOVA and, if significant, with pair-wise Dunn's post-tests. The *p* values of the post-tests were not corrected for multiple comparisons, but Benjamini-Hochberg correction was performed for multiple comparisons among post-tests and the outcomes are listed as statistically significant or not in the column "Sign.?".

SI REFERENCES

1. J. Potworowski, W. Jakuczun, S. Leski, D. Wójcik, Kernel current source density method. *Neural Computation* **24**, 541-575 (2012).
2. R. Oostenveld, P. Fries, E. Maris, J. M. Schoffelen, FieldTrip: Open source software for advanced analysis of MEG, EEG, and invasive electrophysiological data. *Comput Intell Neurosci* **2011**, 156869 (2011).
3. A. M. Amjad, D. M. Halliday, J. R. Rosenberg, B. A. Conway, An extended difference of coherence test for comparing and combining several independent coherence estimates: theory and application to the study of motor units and physiological tremor. *J Neurosci Methods* **73**, 69-79 (1997).
4. I. Perkon, A. Kosir, P. M. Itskov, J. Tasic, M. E. Diamond, Unsupervised quantification of whisking and head movement in freely moving rodents. *J Neurophysiol* **105**, 1950-1962 (2011).
5. N. Rahmati et al., Cerebellar potentiation and learning a whisker-based object localization task with a time response window. *J Neurosci* **34**, 1949-1962 (2014).
6. V. Romano et al., Potentiation of cerebellar Purkinje cells facilitates whisker reflex adaptation through increased simple spike activity. *eLife* **7**, e38852 (2018).